Feasible Thermodynamics Devices Enabled by Thermal-Null Medium

Hooman Barati Sedeh,[1] Mohammad Hosein Fakheri,[1] Ali Abdolali,[1,*] Fei Sun,[2] and Yungui Ma[3]

[1] *Applied Electromagnetic Laboratory, School of Electrical Engineering, Iran University of Science and Technology, Tehran 1684613114, Iran*

[2] *College of Physics and Optoelectronics, Taiyuan University of Technology, Taiyuan 030024, China*

[3] *College of Optical Science and Engineering, Zhejiang University, Hangzhou 310027, China*

(Received 17 May 2020; revised 15 November 2020; accepted 18 November 2020; published 10 December 2020)

Recently, thermal manipulation has gained the attention of the scientific community due to its several applications. In this paper, based on a transformation-thermodynamics methodology, a special type of material, called a thermal-null medium (TNM), is proposed that leads to the design of various thermal functionalities such as thermal bending devices, arbitrarily shaped heat concentrators, and omnidirectional thermal cloaks. In contrast to the conventional transformation-thermodynamics-based conductivities, which are inhomogeneous and anisotropic, TNMs are homogeneous and easy to realize. It is shown that the TNMs obtained are independent of the desired device shape, meaning that if the geometry of the desired device is changed, there is no need to recalculate the conductivities required. This consequently makes the designed devices suitable for scenarios where reconfigurability is of the utmost importance. Several numerical simulations are carried out to demonstrate the capability of TNMs and their application in directional bending devices, concentrators, and cloaks. In order to validate the concept, by using effective-medium theory, a TNM with an aluminum-air multilayer structure is designed and fabricated. The structure realized is then used to implement an elliptically shaped thermal concentrator. It is observed that the experimental results exhibit good agreement with the results obtained from the numerical simulations, which corroborates the effectiveness of the proposed materials.

DOI: 10.1103/PhysRevApplied.14.064034

I. INTRODUCTION

In times of energy shortage, the recycling of heat energy and the manipulation of heat become an important topic. Therefore, how to handle heat dissipation, heat storage, and the control of heat flux has become a significant subject of debate among the scientific community. Various methods have been proposed for achieving this aim, among which transformation thermodynamics (TT) demonstrates high flexibility in the manipulation of heat in an unprecedented manner [1–6]. The main idea of TT is derived from its electromagnetic (EM) counterpart, which was proposed by Pendry *et al.* and named transformation optics (TO) [7]. As analyzed by Pendry's group, an equivalence between Maxwell's equations described in an initial coordinate system (i.e., a virtual domain) and their counterparts in another arbitrary transformed coordinate system (i.e., a physical domain) results in a direct link between the permittivity and permeability of the materials occupying the spaces and the metric tensor of the transformed space, which has the desired EM properties. Soon after the introduction of TO, many novel devices that seemed impossible to achieve with natural materials, such as EM cloaks [8–10], multiemission lenses [11–16], wave concentrators [17–24], and beam splitters [25–27], were proposed. In the same way as the TO methodology, TT has gained much attention due to the intrinsic degree of freedom that it offers. Although TT could pave the way towards designing various devices such as heat cloaks [3,28], heat-flux concentrators [29], and heat-transferring devices [30], it has some serious drawbacks that restrict the usage of this approach in real-life scenarios. The main problem of TT is that the conductivities obtained through this approach are inhomogeneous and anisotropic, which results in difficulties in their fabrication [3]. Although thermal metamaterials have received much attention in recent years, it is still a challenging task to design a thermal cell that possesses both inhomogeneity and anisotropy [31]. In addition to the inhomogeneity problem, the TT-based conductivities are extremely dependent on the input shape of the device. That is, if the geometry of the device is changed, one must not only perform tedious mathematical calculations to obtain the desired conductivities but also redesign the metamaterials, which is time-consuming and not applicable in scenarios where reconfigurability is important. Therefore, for the above-mentioned reasons, one must ask

*abdolali@iust.ac.ir

the question of whether there is any alternative way of designing heat-manipulation devices such that the required conductivities are homogeneous and independent of the input geometry.

In this paper, we propose an alternative method for achieving various thermal devices based on a special type of material called a thermal-null medium (TNM) [32,33]. In contrast to the conventional TT-based conductivities, the TNMs obtained through our approach are homogeneous and geometry free. That is, if the desired device shape is changed, there is no need to recalculate the required conductivities. This makes TNMs a good alternative for use in scenarios where reconfigurability is of the utmost importance. For instance, as the first application of a TNM, a directional heat-bending device is designed such that, regardless of its deflection angle, only one material is used and perfect functionality is achieved. In addition, we use TNMs as a means to obtain arbitrarily shaped heat concentrators using homogeneous materials. It is shown that by utilizing a TNM, one can freely change the geometry of the concentrator while using the same material. Finally, an omnidirectional thermal cloak is proposed that is capable of guiding thermal distributions from any incidence direction in such a manner that they become undetectable to an outside observer. To verify the effectiveness of the proposed material, we implement the TNM with the aid of effective-medium theory (EMT), by utilizing a multilayer structure consisting of 90 layers of aluminum and air in a glass background medium. The realized structure is then used to fabricate an arbitrarily shaped thermal concentrator in order to validate the functionality of the proposed material. It is observed that the experimental results exhibit good agreement with the theoretical predictions and numerical-simulation results.

The rest of this paper is organized as follows. First, the fundamental theoretical formulation of the method is presented, and then several numerical simulations are presented to demonstrate the capability of the proposed approach for achieving different practical functionalities. Next, the experimental verification of the proposed TNM is discussed in detail, and the results of measurements on the fabricated thermal concentrator are analyzed. Finally, the paper ends with a summary of the results obtained.

II. THEORETICAL FORMULATION

The derivation of a TNM is based on a null-space mapping, which is a kind of transformation that results in optical and thermal materials with large anisotropic parameters. Here, we briefly discuss the approach to the derivation; for a more comprehensive study, see Refs. [32,33]. Assume that a slab of width W_v is mapped to another slab of width W_p as shown in Fig. 1.

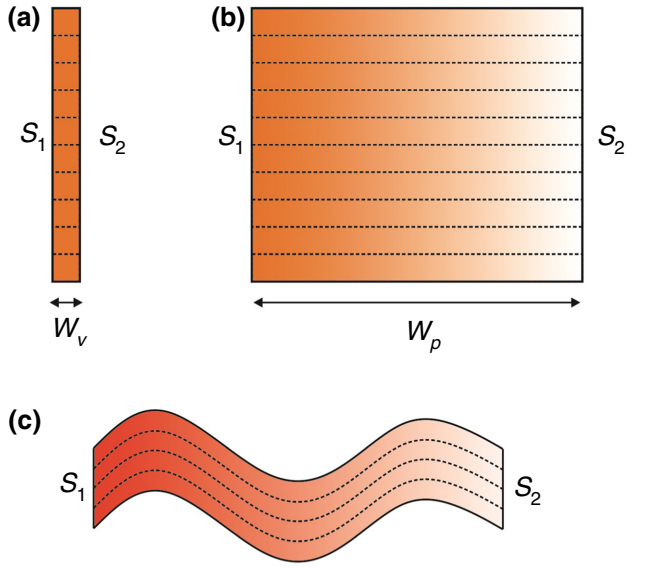

FIG. 1. Schematic diagram of null-space transformation to obtain a TNM. (a) A thin slab in the virtual space is mapped to (b) a slab with a finite thickness. (c) Schematic illustration of a typical shape designed by bending the slab in (b).

The transformation function of such a mapping can be written as

$$x' = \begin{cases} x & x' \in (-\infty, 0], \\ \dfrac{W_p}{W_v} x & x' \in [0, W_p], \\ x - W_v + W_p & x' \in [W_p, \infty). \end{cases} \tag{1}$$

When the thickness of the slab in the virtual space approaches zero (i.e., $W_v \to 0$), its interfaces become very close to each other [see S_1 and S_2 in Fig. 1(a)]. After a null-space transformation [i.e., Eq. (1) when $W_v \to 0$], the thickness of this slab is greatly expanded. To further clarify this concept, assume two arbitrary points x_1 and x_2 in the virtual domain such that their distance from each other is $L = \|x_1 - x_2\|$. After the virtual space is mapped into the physical domain, these points are consequently mapped to x_1' and x_2' with a new distance from each other of $L' = \|x_1' - x_2'\| = (W_p/W_v)\|x_1 - x_2\|$. Since $W_v \to 0$ and W_p has a finite value, then $W_p/W_v \to \infty$, which consequently yields the result that in comparison to the small thickness of slab in the virtual space, the distance between these two points in the physical space approaches to infinity, i.e., $L \to \infty$, unlike the case for the thin slab in the virtual space. Since this discussion is applicable to all points inside the virtual slab, including the ones that are located in the left and right interfaces, the thickness of the virtual slab also expands in the physical space. In other words, while surface S_1 is fixed, surface S_2 is stretched by W_p/W_v times in the physical space, as shown in Fig. 1(b). For a steady-state case, the thermal-conduction equation without a source can be written as $\nabla \cdot (\kappa \nabla T) = 0$, where κ

is the thermal conductivity and T is the temperature. On the other hand, according to the form invariance of the heat-conduction equation under coordinate transformations [3], the thermal-conduction equation in the transformed space can also be written as $\nabla'(\kappa'\nabla' T') = 0$, in which $\kappa' = \Lambda\,\kappa\,\Lambda^T \det(\Lambda)^{-1}$, where $\Lambda = \partial(x', y', z')/\partial(x, y, z)$ is the Jacobian matrix that relates the metrics of the virtual space, (x, y, z), to those of the physical space, (x', y', z'). Therefore, by substituting Eq. (1) into the above relation, the corresponding heat conductivity is obtained as $\kappa' = \mathrm{diag}[W_p/W_v, W_v/W_p, W_v/W_p]$, where diag[·] represents a diagonal matrix. However, because of the null-space transformation (i.e., $W_v \to 0$), the conductivity obtained is changed to

$$\frac{\kappa'}{\kappa} = \begin{bmatrix} \infty & 0 & 0 \\ 0 & 0 & 0 \\ 0 & 0 & 0 \end{bmatrix}. \tag{2}$$

A material obtained by use of Eq. (2) is called a TNM, and is designed by use of a null-space transformation. Since the thermal resistance is inversely proportional to the thermal conductivity, $R_{\parallel} \to 0$ and $R_{\perp} \to \infty$, which leads to a supertransferring performance along the "stretching" direction without dissipation. In other words, the function of the TNM is to guide heat very fast along its main stretching direction (i.e., $\hat{x}$) and extremely slowly in other directions (i.e., $\hat{y}$ and $\hat{z}$). Besides, as was comprehensively discussed in Ref. [32,33], TNMs are not restricted to a Cartesian coordinate system. In fact, TNMs of any other shape can be obtained by bending the slab in Fig. 1(b) and still guide the thermal field directionally without any dissipation, as shown in Fig. 1(c). It is worth mentioning that although the concept of a null transformation has been previously introduced in other areas of physics such as electromagnetism, acoustics, and electrostatics [22,24,34–40], this paper extends it into the realm of thermal science for achieving different functionalities.

III. NUMERICAL SIMULATIONS

To verify the correctness and effectiveness of the proposed TNM, directional heat-bending devices are analyzed as the first example by performing simulations, which are carried out using the COMSOL Multiphysics finite-element solver. Figure 2 demonstrates the primary goal of our design. As can be seen, there is a need to change the direction of heat flow by an angle α.As shown in Fig. 2, an interface at a higher temperature is separated from one at a lower temperature, with a deflection angle α. The input surface (which has the higher temperature, T_H) and the output surface (which has the lower temperature, T_C) are labeled S_1 and S_2, respectively. It is clear from Fig. 2 that a common plane S (shown in red) can be obtained if one extends the edges of surfaces S_1 and S_2 (indicated by black dashed lines). According to the above discussion, filling the region between surfaces S_1 and S with a TNM with its main axis along the $\hat{x}$ direction (i.e., $\kappa_x \to \infty$ and $\kappa_y \to 0$) and the area between surfaces S and S_2 with a TNM with its main axis along the u direction (which is rotated by an angle α with respect to the $\hat{x}$ direction) results in a point-to-point mapping and, in turn, gives rise to bending of the heat distribution directionally from S_1 to S_2. In other words, the surfaces S_1, S_2, and S are all equivalent surfaces, in such a manner that heat distributions on S_1 are first projected onto S along the $\hat{x}$ direction and then projected onto S_2 along the α direction. Note that the entire design process is general, without the need for any mathematical calculations, and is valid for any arbitrary deflection angle α. To demonstrate such a capability, several thermal bending devices with different bending angles and structures are simulated, and the results are depicted in Fig. 3.

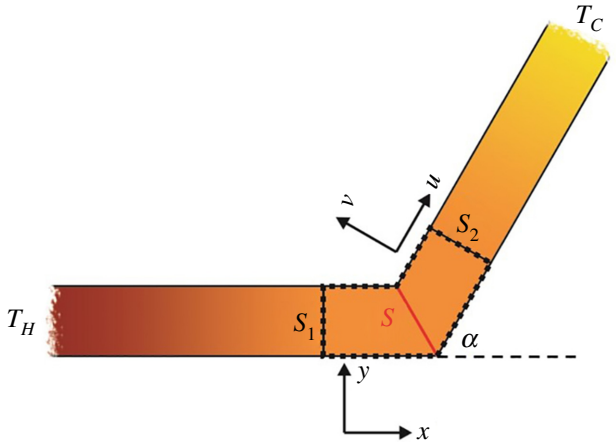

FIG. 2. Schematic transformation for describing a directional heat-bending device.

In the simulations, Dirichlet boundary conditions are applied at the input and output surfaces. That is, the temperature of the input surface is set to $T_H = 315$ K, while $T_C = 275$ K is assigned to the output interface. Neumann boundary conditions are applied to the rest of the boundaries, which act as thermal insulation, to avoid any other effects and to demonstrate only the functionality of the material utilized. As can be seen from Figs. 3(a) and 3(b), the TNM obtained is capable of connecting two thermal surfaces with any desired deflection angle, without any deviation in their thermal contours. This makes it a suitable material for use in scenarios where reconfigurability is of the utmost importance or there is a requirement to manipulate heat distributions directionally along an arbitrary path, as shown in Fig. 3(c). Furthermore, according to Fig. 3(d), the fictitious surface S can also be located in a cylindrical coordinate system (i.e., along the azimuthal direction $\hat{\phi}$) rather than in a Cartesian coordinate system, and its functionality remains unchanged.

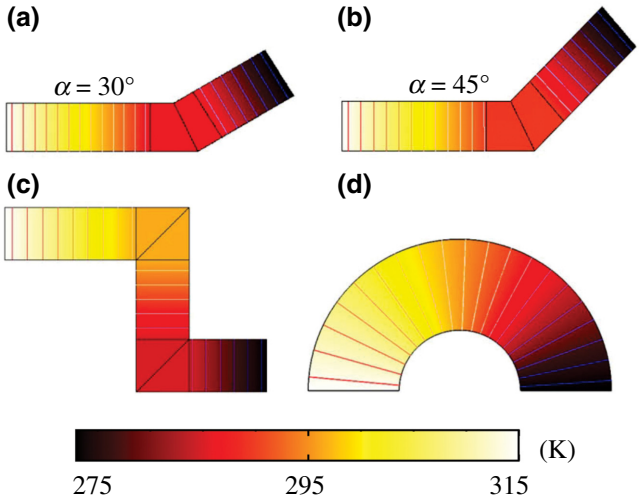

FIG. 3. Thermal distributions in heat-bending devices with different bending angles (a) $\alpha = 30^\circ$ and (b) $\alpha = 45^\circ$, and with the TNM in (c) a Cartesian and (d) a cylindrical coordinate system.

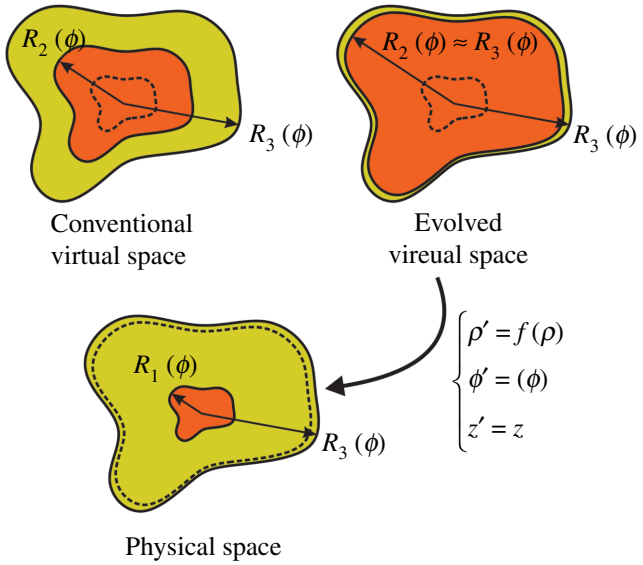

FIG. 4. Schematic illustration of coordinate transformation for achieving arbitrarily shaped concentrators.

In addition to directional thermal bending devices, much more attention has been paid to renewable energy over the last few decades, since fossil fuels are being depleted. Among all the proposed methods, solar energy has been widely exploited as one of the most important types of renewable energy, for converting energy from the Sun to electricity. In general, the conversion of solar energy to electricity is performed via two approaches, namely direct solar-electrical energy conversion and indirect conversion. In the one specified in Eq. (10), solar-cell devices are used, while in the material describing of Eq. (11), thermal energy is used as a mediator by employing a device called a solar thermal collector (STC). Heat-flux concentrators are an example of the second group (i.e., STCs) that have received a lot of attention in the past decade. Recently, the TT method has been extended to manipulate heat currents and localize thermal energy using heat-flux concentrators. However, the conventional challenges of the TT-based conductivities (i.e., inhomogeneity and shape dependency) are still the main drawback of this approach, and restrict its applicability in practical situations and are yet to be addressed. Nevertheless, by extending the idea of a null-space transformation, one can exploit TNMs as a means of collecting thermal energy in any arbitrary region of interest. To this end, the space transformation shown in the schematic diagram in Fig. 4 is used, in which three cylinders with arbitrary cross sections $R_1(\phi) = \tau_1 R(\phi)$, $R_2(\phi) = \tau_2 R(\phi)$, and $R_3(\phi) = \tau_3 R(\phi)$ divide the space (i.e., the virtual space) into three different regions. It should be noted that $R(\phi)$ is an arbitrary continuous function with a period of 2π that is specified by a Fourier series and defines the cross section of the concentrator.

To concentrate the thermal energy into a predefined region $R_1(\phi)$, one must collect the energy that was originally located in $\rho < R_2(\phi)$ into the region $\rho' < R_1(\phi')$, as shown in Fig. 4. To achieve this aim, as explained in Ref. [3,31], the region $\rho \in [0, R_2(\phi)]$ must be compressed into the region $\rho' \in [0, R_1(\phi')]$, while at the same time $\rho \in [R_2(\phi), R_3(\phi)]$ is stretched into the region $\rho' \in [R_1(\phi'), R_3(\phi')]$. Since these two steps occur simultaneously, all the energy that was previously located in $\rho < R_2(\phi)$ is now localized in the region $\rho' < R_1(\phi')$, and, as a result, the thermal intensity is increased in this domain.

The function that is able to perform such a transformation can be expressed as

$$\begin{cases} f_c(\rho,\phi) = \dfrac{\tau_1}{\tau_2}\rho & \rho' \in [0, R_1(\phi)), \\ f_s(\rho,\phi) = \chi\rho + \Theta R(\phi) & \rho' \in [R_1(\phi), R_3(\phi)], \end{cases} \tag{3}$$

where the subscripts c and s represent the compressed and stretched regions, respectively, $\chi = (\tau_3 - \tau_1)/(\tau_3 - \tau_2)$, and $\Theta = [(\tau_1 - \tau_2)/(\tau_3 - \tau_2)]\tau_3$. Thus, according to the TT methodology, the materials required for each region can be achieved as follows:

$$\frac{\kappa_c'}{\kappa_0} = \begin{bmatrix} 1 & 0 & 0 \\ 0 & 1 & 0 \\ 0 & 0 & (\tau_2/\tau_1)^2 \end{bmatrix}, \quad \frac{\kappa_s'}{\kappa_0} = \begin{bmatrix} m_{11} & m_{12} & 0 \\ m_{21} & m_{22} & 0 \\ 0 & 0 & m_{33} \end{bmatrix}, \tag{4}$$

where the coefficients m_{ij} are

$$\begin{aligned} m_{11} &= \frac{(\tau_3-\tau_2)\rho' - \tau_3(\tau_1-\tau_2)R(\phi)}{(\tau_3-\tau_2)\rho'} \\ &\quad + \frac{\tau_3^2(\tau_1-\tau_2)^2[dR(\phi)/d\phi]^2}{[(\tau_3-\tau_2)^2\rho' - \tau_3(\tau_1-\tau_2)(\tau_3-\tau_2)R(\phi)]\rho'}, \\ m_{12} &= m_{21} = \frac{[\tau_3(\tau_1-\tau_2)(dR/d\phi)]}{(\tau_3-\tau_2)\rho' - \tau_3(\tau_1-\tau_2)R(\phi)}, \\ m_{22} &= \frac{(\tau_3-\tau_2)\rho'}{(\tau_3-\tau_2)\rho' - \tau_3(\tau_1-\tau_2)R(\phi)}, \\ m_{33} &= \frac{(\tau_3-\tau_2)^2\rho' - \tau_3(\tau_1-\tau_2)(\tau_3-\tau_2)R(\phi)}{(\tau_3-\tau_1)^2\rho'}. \end{aligned} \tag{5}$$

As can be seen from Eqs. (4) and (5), the materials obtained in the stretched region are inhomogeneous and anisotropic, with off-diagonal components m_{12} and m_{21}, which cause serious difficulties in their realization. In fact, the reason why no experimental verification of arbitrarily shaped thermal concentrators has yet been proposed is due to the existence of these inhomogeneous and off-diagonal components. In addition to the inhomogeneity that the presence of $R(\phi)$ in the components m_{ij} dictates, this also demonstrates the dependency of the materials obtained on the geometry of the structure. In other words, an alteration in the cross section of the concentrator [i.e., $R(\phi)$] leads to new materials, which must be recalculated. However, since $R_2(\phi) = \tau_2 R(\phi)$ is a fictitious region, τ_2 can have any arbitrary value. This gives us a degree of freedom to arbitrarily select the value of τ_2 in such a manner that it eradicates the effect of the off-diagonal components m_{12} (and also m_{21}). Therefore, without loss of generality, one can assume that $\tau_2 \to \tau_3$ (a null-space transformation). By setting such a value for τ_2, the coefficients of Eq. (5) are obtained as follows:

$$\begin{cases} m_{11} = 1/\Delta, \\ m_{12} = m_{21} = -\kappa_0 \dfrac{dR(\phi)/d\phi}{R(\phi)}, \\ m_{22} = m_{33} = \Delta, \end{cases} \tag{6}$$

whence $\Delta \to 0$. As can be seen from Eq. (6), the conductivities obtained still suffer from anisotropy and inhomogeneity problems due to the existence of m_{12} (and also m_{21}) and their dependence on the shape of the contour of $R(\phi)$. However, it is known that in the absence of a heat source the steady-state heat-diffusion equation is governed by the Laplace equation as follows:

$$\nabla \cdot (\bar{\bar{\kappa}}\, \nabla T) = \sum_{j,k=1}^{n} \frac{\partial^{j,k}}{\partial x^j} \kappa \frac{\partial T}{\partial x^k} = 0. \tag{7}$$

Therefore, by substituting Eq. (6) into Eq. (7), the Laplace equation in cylindrical coordinates is obtained:

$$\begin{aligned} &\frac{1}{\rho}\partial T/\partial\rho + \partial^2 T/\partial\rho^2 + \frac{2}{\rho} m_{12}\Delta\, \partial^2 T/\partial\rho\, \partial\phi \\ &\quad + \frac{1}{\rho}\frac{\partial m_{12}}{\partial\phi}\Delta\, \partial T/\partial\rho + \frac{1}{\rho^2}\Delta^2\, \partial^2 T/\partial\phi^2 \\ &\quad + \Delta^2\, \partial^2 T/\partial z^2 = 0. \end{aligned} \tag{8}$$

Since $\Delta \to 0$ and m_{12} has a finite value according to Eq. (6), the exact value of m_{12} is not important. This is because only the products of these values, not each of them individually, play a crucial role, as shown in the Laplace equation [i.e., Eq. (8)]. Therefore, one can assume any desirable finite value for the off-diagonal components. Here we assume $m_{12} = 0$; this assumption eradicates the off-diagonal components of Eq. (6).

Hence, the final conductivities, which describe the performance of an arbitrarily shaped thermal concentrator, are obtained as follows:

$$\frac{\kappa_c'}{\kappa_0} = \begin{bmatrix} 1 & 0 & 0 \\ 0 & 1 & 0 \\ 0 & 0 & (\tau_2/\tau_1)^2 \end{bmatrix}, \quad \frac{\kappa_s'}{\kappa_0} = \begin{bmatrix} \infty & 0 & 0 \\ 0 & 0 & 0 \\ 0 & 0 & 0 \end{bmatrix}. \tag{9}$$

To validate the concept, several arbitrarily shaped concentrators are simulated. The solution area consists of a square, where there is a planar metallic plate at the position $x = -0.3$ m with a temperature $T = 315$ K, and another metallic plate at $x = +0.3$ m with a temperature $T = 275$ K. In all the simulations performed, it is assumed that the values $\tau_1 = 0.5$, $\tau_2 = 0.99$, and $\tau_3 = 1$ are constant, while $R(\phi)$ is changed for each new case. The first example is concerned with concentrators of circular and elliptical cross section, and the results are illustrated in Fig. 5. As can be seen from Figs. 5(a) and 5(b), the thermal concentrator does not change the thermal distribution, and this agrees well with the theoretical investigations. In addition, since at a specific location in the background medium the heat flux is equal to 350 W/m^2, it is expected that at this particular location, the heat flux will be enhanced by a factor of $\tau_2/\tau_1 = 1.98$. This is verified by the numerical simulations, as shown in Figs. 5(c) and 5(d). It is evident that in the compressed region the heat flux is increased from 350 to 693 W/m^2, which is in good agreement with the theoretical predictions.

To have full control of the heat flux, it may be necessary in some cases that the thermal energy is localized in a certain domain with an arbitrary cross section. To date, no systematic proposal for achieving an arbitrarily shaped thermal concentrator has been made. As previously mentioned, the method presented in this paper results in anisotropic conductivities that are independent of the geometry of the concentrator. That is, the conductivities

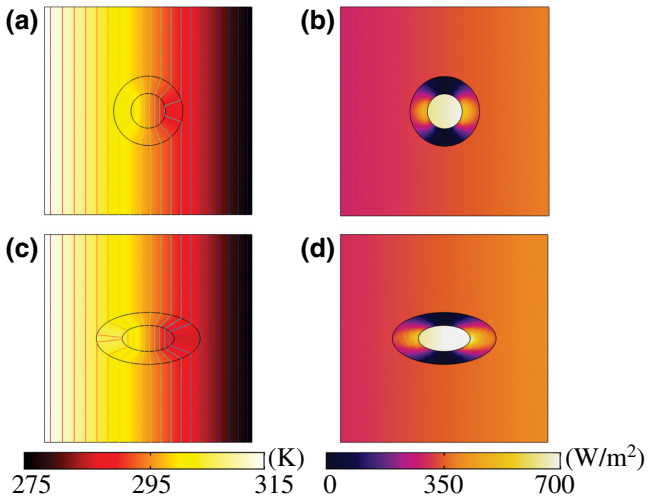

FIG. 5. Results for the temperature distribution in heat-flux concentrators with different cross sections: (a) circular, (b) elliptical. (c),(d) Corresponding thermal flows.

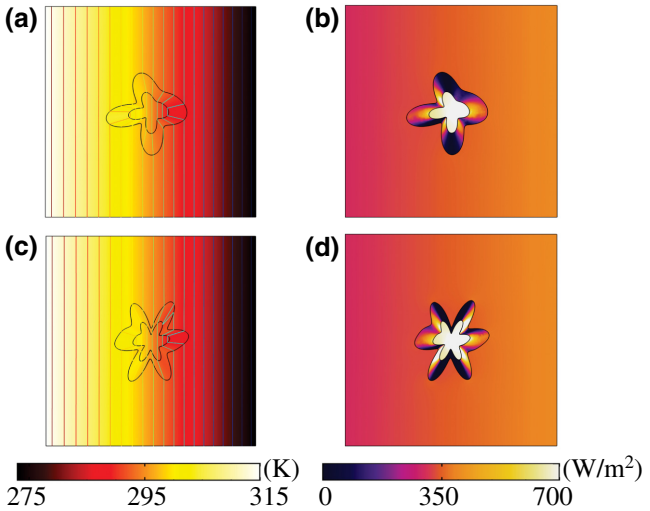

FIG. 6. (a),(b) Results for the temperature distribution in heat-flux concentrators with arbitrary cross sections. (c),(d) Corresponding thermal flows.

obtained from Eq. (9) are sufficient for any desired geometry. This, in turn, makes the proposed approach a good candidate for scenarios where reconfigurability is of the utmost importance. To show this, $R(\phi)$ is changed in such a way that an arbitrarily shaped concentrator is generated. By utilizing the conductivities obtained for each compressed and stretched region, the results shown in Fig. 6 are obtained for the thermal flux and temperature distribution.

As shown in Figs. 6(a) and 6(b), in the same way as in the previous case, the isothermal lines do not deviate in the background medium, which indicates that the designed thermal concentrator does not affect the thermal distribution. Moreover, according to Figs. 6(c) and 6(d), in the new scenario the thermal flow is increased from 350 to 693 W/m^2 in the compressed region without any distortion in its temperature distribution. However, it is worth mentioning that changing the ratio τ_2/τ_1 results in different values for the thermal energy inside the compressed domain. Moreover, it should be emphasized that the previously reported coordinate-transformation (CT)-based materials have a strict dependency on the shape of the corresponding devices and the constitutive parameters of the background medium in which the device is located. In other words, if the shape of the concentrator is changed, one needs to recalculate and redesign the materials required, in order to have perfect functionality. This consequently makes the previous approaches impractical for use in scenarios where adaptability is of the utmost importance. Nevertheless, according to the results given in Figs. 5 and 6, it is clear that the TNM is independent of the device shape. That is, after the TNM has been designed, changing the shape of the concentrator does not affect its performance.

As the final example, a square-shaped heat-flux cloak is proposed, constructed via the utilization of a TNM. To date, no systematic proposal that yields an omnidirectional heat cloak has been made. In this paper, we propose a square-shaped cloak that is capable of guiding thermal distributions in such a manner that an object becomes undetectable to an outside observer. Since heat diffuses from a higher-temperature region to a lower-temperature one, if an obstacle is located in the path of the thermal flux, a distortion in the isothermal lines will occur and, in turn, give rise to a degradation of the performance efficiency. However, when a square-shaped heat cloak is used, this cloak allows the heat flux to pass smoothly around the cloaked region without creating any distortion, as shown schematically in Fig. 7(a). To design such a cloak based on the CT methodology, the transformation function shown in Fig. 7(b) is used. In contrast to previously reported cloaks, which mapped a point in the virtual space into a circle in the physical space, here the cloak region is divided into different regions and, in each domain, a linear transformation function is exploited. The space between a square with a side length L (i.e., $ABCD$) in the virtual space is transformed to the same square with the same side length in the physical space (i.e., $A'B'C'D'$), while at the same time an inner square with a side length ℓ_1 (i.e., $EFGH$) in the virtual space is mapped to a larger square with a side length ℓ_2 (i.e., $E'F'G'H'$) in the physical space.

Without loss of generality, one can assume that the side length of the inner square approaches zero (i.e., $\ell_1 \to 0$). Therefore, under this assumption, the triangles $\triangle OAB$, $\triangle OBC$, $\triangle OCD$, and $\triangle ODA$ in the virtual space [Fig. 7(b)] are transformed to triangles $\triangle F'A'B'$, $\triangle G'B'C'$, $\triangle H'C'D'$, and $\triangle E'D'A'$, respectively, in the physical space.

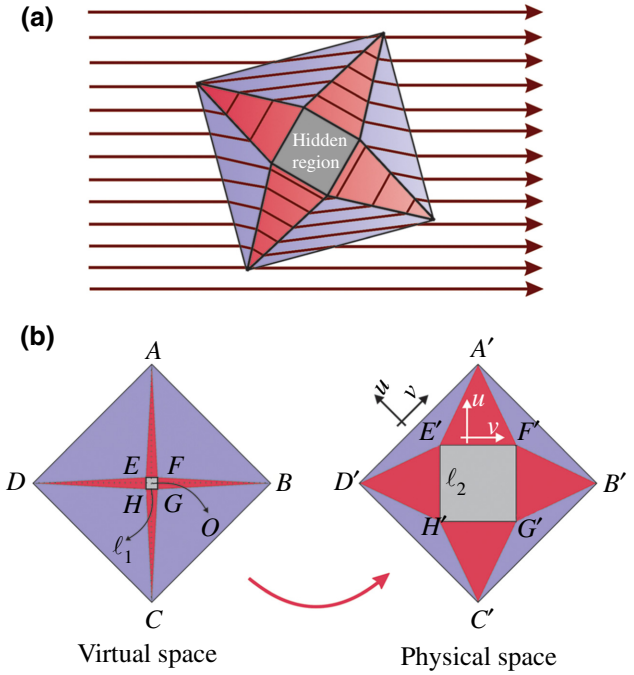

FIG. 7. (a) Schematic illustration of the heat-flux path when a TT-based cloak is utilized. (b) Mapping function required for designing a square-shaped cloak.

Meanwhile, the lines AO, BO, CO, and DO in the virtual space must also be transformed to triangles $\triangle A'E'F'$, $\triangle B'F'G'$, $\triangle C'G'H'$, and $\triangle D'H'E'$, respectively, in the physical space. As a result of these mappings, the object that is to be cloaked does not affect the heat distribution and will be invisible to an outside detector. By introducing a local coordinate system for each of the pink triangular regions ($\triangle D'H'E'$ and $\triangle B'F'G'$, denoted below by I and III, respectively, and $\triangle A'E'F'$ and $\triangle C'G'H'$, denoted by II and IV, respectively), we obtain the required conductivities for each of these regions:

$$\frac{\kappa'_{\mathrm{I,III}}}{\kappa_0} = \begin{bmatrix} 0 & 0 & 0 \\ 0 & \infty & 0 \\ 0 & 0 & 0 \end{bmatrix}, \quad \frac{\kappa'_{\mathrm{II,IV}}}{\kappa_0} = \begin{bmatrix} \infty & 0 & 0 \\ 0 & 0 & 0 \\ 0 & 0 & 0 \end{bmatrix}. \quad (10)$$

In addition, the conductivities of the remaining regions (denoted by the subscript R) in their local coordinate system [i.e., (u, v, z)] are also obtained:

$$\frac{\kappa'_R}{\kappa_0} = \begin{bmatrix} \frac{1}{\Gamma} & 0 & 0 \\ 0 & \Gamma & 0 \\ 0 & 0 & \frac{1}{\Gamma} \end{bmatrix}, \quad (11)$$

where $\Gamma = 1 - (\sqrt{2}l_2/L)$. Compared with previous prototype cloaks with extremely inhomogeneous and anisotropic material parameters, the square cloak is simplified to one

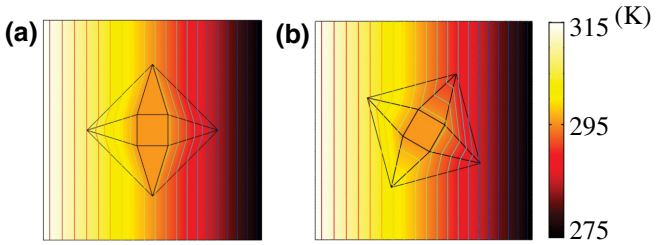

FIG. 8. Heat-flux distributions when the designed square-shaped cloak is used with different incidence angles (a) $\theta = 0^\circ$ and (b) $\theta = 15^\circ$.

containing only two homogeneous materials. One of these materials has a simple diagonal anisotropic conductivity tensor, which could be easily implemented via a thermal metamaterial [31,41], and the other is the TNM that is introduced in this paper. To demonstrate the effectiveness of the proposed cloak, we simulate it using the conductivities given in Eqs. (10) and (11) for each of the corresponding regions with two different angles $\theta_{\mathrm{inc}} = 0^\circ$ and $\theta_{\mathrm{inc}} = 15^\circ$, and the results are shown in Fig. 8.

As can be seen from Fig. 8(a), the isothermal contours pass the object smoothly without any distortion. Moreover, in contrast to previous cloaks, when the incidence angle is changed, the functionality of the cloak designed here remains unchanged, as shown in Fig. 8(b). In other words, the functionality of the cloak presented here is not restricted to any specific incidence angle.

IV. EXPERIMENTAL VERIFICATION

Although the proposed method is capable of resulting in various functionalities using only one constant homogeneous material, the challenging question is how such a TNM could be implemented in real-life scenarios.

To answer this question, we take advantage of EMT and validate the functionality of the proposed material by realizing the elliptically shaped thermal concentrator shown in Fig. 5(c). According to EMT, a multilayer structure of the kind shown in Fig. 9(a), such that its constituent layers have isotropic thermal properties κ_A and κ_B, can lead to an effective anisotropic conductivity with the parameters

$$\kappa_x = \kappa_A f + \kappa_B(1-f), \quad \frac{1}{\kappa_y} = \frac{f}{\kappa_A} + \frac{(1-f)}{\kappa_B}, \quad (12)$$

where κ_x and κ_y are the effective anisotropic thermal conductivities orthogonal and parallel, respectively, to the direction of the interface between the two isotropic media, and $f = d_A/(d_A + d_B)$ is the filling fraction of the first material.

In order to design the TNM, we use aluminum ($\kappa_A = 205$ W/m K) as the first material and air ($\kappa_B = 0.026$ W/m K) as the second material, and the whole multilayer structure is embedded in a glass background with

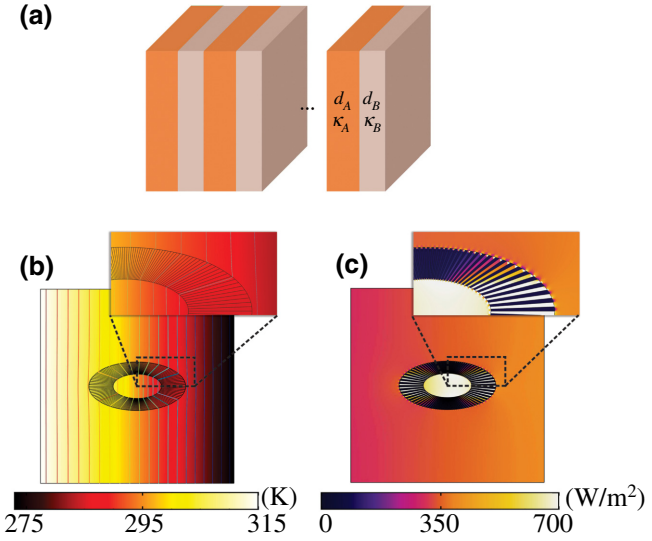

FIG. 9. (a) A multilayer system that mimics the behavior of an anisotropic slab. (b) Results for the temperature distribution in a multilayer heat-flux concentrator. (c) Corresponding thermal flow. The inset shows the details of the layered structure.

a thermal conductivity $\kappa_G = 1.05$ W/m K. Substituting these parameters into Eq. (12) and selecting the filling fraction $f = 0.5$ consequently gives rise to $\kappa_x = 102.513$ W/m K and $\kappa_y = 0.052$ W/m K. The effective conductivities obtained correspond to $\kappa_x/\kappa_G = 97.63$ and $\kappa_y/\kappa_G = 0.0495$ compared with the conductivity of the background. It should be remarked that an ideal TNM has components $\kappa_\rho/\kappa_G = \infty$ and $\kappa_\phi/\kappa_G = 0$, which means that the static heat equation in such a medium can be expressed as $\partial^2 T/\partial\rho^2 + (1/\rho)\partial T/\partial\rho = 0$. As can be deduced from the equation obtained, in an ideal TNM, the geometrical variations in the azimuthal direction vanish, which confirms the applicability of TNMs in arbitrarily shaped concentrators.

However, since obtaining these exact extreme values in the real world, as well as in the experimental setup, is impossible, we have to make some approximations. For this purpose, we assume $\kappa_\rho/\kappa_G = 1/\Delta$ and $\kappa_\phi/\kappa_G = \Delta$, where $\Delta \to 0$, which consequently leads the governing heat equation to be obtained as $\partial^2 T/\partial\rho^2 + (1/\rho)\partial T/\partial\rho + (\Delta^2/\rho^2)(\partial^2 T/\partial\phi^2) = 0$. Comparing the two equations obtained clearly demonstrates that the closer to zero the value of Δ realized (hereafter expressed as Δ_R) is, the more similar the governing equation becomes to that corresponding to the ideal case. In other words, for smaller values of Δ_R, the material implemented mimics better the behavior of an ideal TNM. For the values selected, $\Delta_R \approx 5 \times 10^{-4}$, which is small enough to be neglected and leads the heat equation in the medium implemented to be the same as in the ideal case. Therefore, from the above points, it can be understood that the approximation made is reasonably valid, and thus the proposed combination of materials can mimic the behavior of a TNM. It is worth mentioning that according to Eq. (9), the conductivity of the compressed region is $\kappa_c' = \kappa_0\,\mathrm{diag}[1, 1, 3.92]$. Since we are solving the problem for a two-dimensional case, the effective conductivity that is required to be realized in this domain is $\kappa_r^c = \kappa_\phi^c = \kappa_0$. This suggests that instead of using a multilayer structure for the compressed region, one can use a material that is the same as the background medium, which clearly eases the fabrication process. To verify the correctness of the materials obtained, the elliptically shaped thermal concentrator shown in Fig. 5(c) is realized, and the results are demonstrated in Figs. 9(b) and 9(c).

As is depicted in Fig. 9(b), the materials utilized do not cause any distortion in the temperature distribution in the designed concentrator. In addition, as can be seen from Fig. 9(c), the thermal flow is increased from 350 to 693 W/m^2 in the compressed region. Therefore, the materials utilized can mimic the behavior of an ideal TNM and thus lead to almost perfect functionality. We emphasize that the performance of the designed TNM is independent of the device geometry, and the same realized material as that used in Fig. 9 could also be exploited for other shapes and the results would not change.

Hence, in accordance with the above points, and utilizing an aluminum-air multilayer structure for the stretched region, the final schematic configuration obtained for the thermal concentrator is as shown in Fig. 10(a). As shown in this figure, we use two containers, one filled with hot water as a source and the other filled with cold water as a sink. The temperature distributions are then monitored by a thermography camera, which is fixed above the structure. A sample corresponding to the case shown in Fig. 9(b) is fabricated with the given material, and a photograph is shown in Fig. 10(b). The stretched region of the elliptically shaped concentrator consists of 90 alternating wedge-shaped aluminum and air layers with the filling fraction given above. That is, the share of each material is 45 layers each, with an angle of 4°. As previously mentioned, the same material as the background medium is also used for the compressed region. The whole structure is cast into a rectangular-shaped glass background of side length 150 × 120 mm^2. In the experimental setup, the left boundary of the glass medium is placed in cold water, which acts as a sink with a constant temperature of 7 °C (280.15 K), while the right boundary is placed in hot water at a constant temperature of 68 °C (341.15 K), which acts as a source. The fabricated sample is then placed in a vacuum chamber. Since there is no air in a vacuum, convection does not happen, and one can safely consider the effects of conduction only. It is worth mentioning that conduction in a vacuum occurs only between objects that are touching. As different parts of the concentrator are attached together in the case presented in this paper, conduction will undoubtedly occur in the vacuum chamber, and the concentrator's performance can be analyzed in such a chamber.

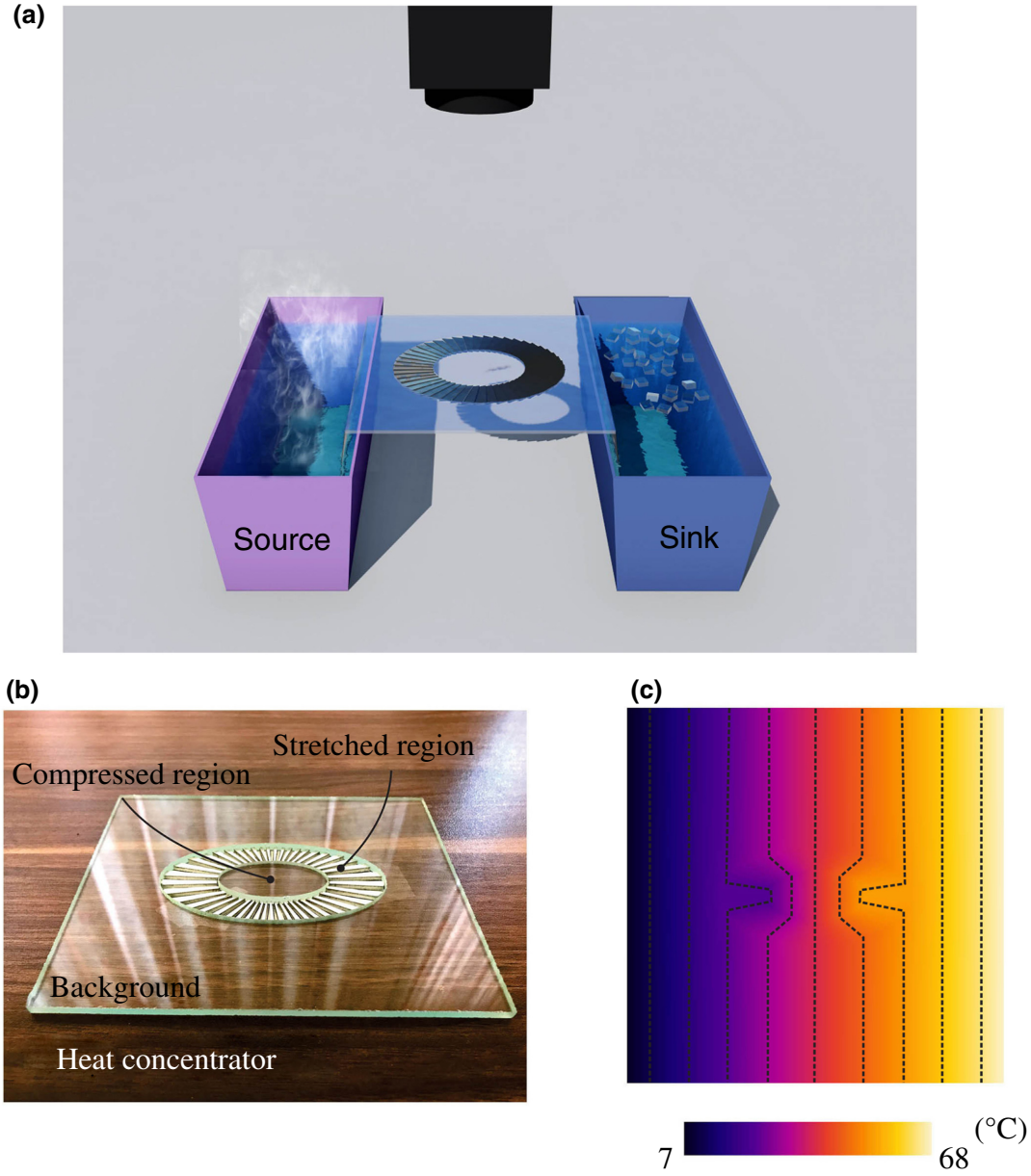

FIG. 10. (a) Schematic configuration of the experimental setup for achieving a thermal concentrator. (b) Photograph of the fabricated elliptically shaped thermal concentrator. (c) Corresponding experimental results for the temperature distribution.

This configuration generates two line-shaped thermal sources, which agree well with the sources utilized in the numerical simulations. The temperature profile in the implemented concentrator is recorded by an infrared camera (OLIP, model ThermoCam p200). The results for the measured temperature distribution are shown in Fig. 10(c). As can be seen from this figure, the compressed region attracts isothermal lines, which indicate an increase in the heat-flux density inside the elliptical region. The experimental results exhibit good agreement with the numerical-simulation results given in Fig. 9(b). More importantly, the temperature gradients outside the stretched region are almost uniform, as predicted by the simulation results and theoretical predictions. In particular, for any thermal device to function thermally in a background medium and not perturb the external thermal profile, the thermal conductivity of the background material should be close to the reduced average of those of the two constituent materials, that is, $\kappa_b = \sqrt{\kappa_A \kappa_B} \approx 2$ W/m K [42]. We select glass as the background medium, with a thermal conductivity $\kappa_G = 1.05$ W/m K. The difference in thermal conductivity between glass and the ideal background medium is not large, which may lead to a small but nonzero interfacial heat transfer. Moreover, since we measure a static thermal

effect, the influence of the small mismatch of the thermal contact resistance is not obvious.

Hence, according to the above points, it can be understood that the proposed materials can approximately mimic the behavior of an ideal TNM, thus making the fabricated sample capable of localizing the heat flux in any desired area with only a slight disturbance of the temperature profile of the background. In addition, the proposed materials are independent of the device geometry. That is, not only can one easily exploit the same constituent materials as in Fig. 1(b) for another arbitrarily shaped thermal concentrator and yet achieve perfect functionality, but they can also be used for the other applications presented in this paper.

V. CONCLUSION

In conclusion, in this paper we present an approach based on a null-space transformation that is capable of obviating the conventional challenges of the TT methodology. The material obtained by the method presented, which is called a TNM, has a homogeneous and anisotropic conductivity that is independent of the device shape. In other words, when the geometry of the structure (e.g., the deflection angle of a directional heat device) is changed, the same material can be used again without the need for recalculating or refabricating it. This, in turn, makes the proposed material a good candidate for use in more practical scenarios. Several numerical simulations are presented, which corroborate the validity and effectiveness of the proposed approach. As the first example, a directional heat-bending device is designed based on a constant TNM, and perfect functionality is obtained despite its deflection angle. In addition to the bending device, we use a TNM as a means to obtain arbitrarily shaped heat concentrators using homogeneous materials. It is shown that by utilizing a TNM, one can freely change the geometry of the concentrator and still use the same material. As another interesting application, an omnidirectional thermal cloak is also proposed that is capable of guiding thermal distributions in such a manner that an object becomes undetectable to an outside observer. To validate the proposed material, we use EMT to realize a TNM with a multilayer structure consisting of 90 aluminum-air layers in a glass background medium. Then, the implemented structure is used in order to fabricate an elliptically shaped thermal concentrator. It is observed that the experimental results exhibit good agreement with the theoretical predictions and numerical-simulation results, which corroborates the correctness of the design procedure.

[1] C. Fan, Y. Gao, and J. Huang, Shaped graded materials with an apparent negative thermal conductivity, Appl. Phys. Lett. **92**, 251907 (2008).

[2] T. Chen, C.-N. Weng, and J.-S. Chen, Cloak for curvilinearly anisotropic media in conduction, Appl. Phys. Lett. **93**, 114103 (2008).

[3] S. Guenneau, C. Amra, and D. Veynante, Transformation thermodynamics: Cloaking and concentrating heat flux, Opt. Express **20**, 8207 (2012).

[4] R. Schittny, M. Kadic, S. Guenneau, and M. Wegener, Experiments on Transformation Thermodynamics: Molding the Flow of Heat, Phys. Rev. Lett. **110**, 195901 (2013).

[5] Y. Liu, W. Jiang, S. He, and Y. Ma, An efficient plate heater with uniform surface temperature engineered with effective thermal materials, Opt. Express **22**, 17006 (2014).

[6] Y. Ma, L. Lan, W. Jiang, F. Sun, and S. He, A transient thermal cloak experimentally realized through a rescaled diffusion equation with anisotropic thermal diffusivity, NPG Asia Mater. **5**, e73 (2013).

[7] J. B. Pendry, D. Schurig, and D. R. Smith, Controlling electromagnetic fields, Science **312**, 1780 (2006).

[8] R. Liu, C. Ji, J. Mock, J. Chin, T. Cui, and D. Smith, Broadband ground-plane cloak, Science **323**, 366 (2009).

[9] L. Xu and H. Chen, Conformal transformation optics, Nat. Photonics **9**, 15 (2015).

[10] M. H. Fakheri, H. Barati, and A. Abdolali, Carpet cloak design for rough surfaces, Chin. Phys. Lett. **34**, 084101 (2017).

[11] P.-H. Tichit, S. N. Burokur, and A. de Lustrac, Spiral-like multi-beam emission via transformation electromagnetics, J. Appl. Phys. **115**, 024901 (2014).

[12] K. Zhang, X. Ding, D. Wo, F. Meng, and Q. Wu, Experimental validation of ultra-thin metalenses for n-beam emissions based on transformation optics, Appl. Phys. Lett. **108**, 053508 (2016).

[13] H. Barati, Z. Basiri, and A. Abdolali, Acoustic multi emission lens via transformation acoustics, Chin. Phys. Lett. **35**, 104301 (2018).

[14] Z. H. Jiang, M. D. Gregory, and D. H. Werner, Broadband high directivity multibeam emission through transformation optics-enabled metamaterial lenses, IEEE Trans. Antennas Propag. **60**, 5063 (2012).

[15] A. Ashrafian, M. H. Fakheri, and A. Abdolali, Space wave channeling enabled by conformal transformation optics, JOSA B **36**, 2499 (2019).

[16] H. Barati, M. H. Fakheri, and A. Abdolali, Exploiting transformation optics for arbitrary manipulation of antenna radiation pattern, IET Microw. Antennas Propag **39**, 1271 (2019).

[17] M. Rahm, D. Schurig, D. A. Roberts, S. A. Cummer, D. R. Smith, and J. B. Pendry, Design of electromagnetic cloaks and concentrators using form-invariant coordinate transformations of Maxwell's equations, Photonics Nanostruct. **6**, 87 (2008).

[18] J. Yang, M. Huang, C. Yang, Z. Xiao, and J. Peng, Metamaterial electromagnetic concentrators with arbitrary geometries, Opt. Express **17**, 19656 (2009).

[19] M. Sadeghi, S. Li, L. Xu, B. Hou, and H. Chen, Transformation optics with Fabry-Pérot resonances, Sci. Rep. **5**, 8680 (2015).

[20] P.-F. Zhao, L. Xu, G.-X. Cai, N. Liu, and H.-Y. Chen, A feasible approach to field concentrators of arbitrary shapes, Front. Phys. **13**, 134205 (2018).

[21] C. F. Yang, M. Huang, J. J. Yang, T. H. Li, F. C. Mao, and P. Li, Arbitrarily shaped homogeneous concentrator and its layered realization, Opt. Commun. **435**, 150 (2019).
[22] M. H. Fakheri, A. Abdolali, and H. B. Sedeh, Arbitrary Shaped Acoustic Concentrators Enabled by Null Media, Phys. Rev. Appl. **13**, 034004 (2020).
[23] M.-Y. Zhou, L. Xu, L.-C. Zhang, J. Wu, Y.-B. Li, and H.-Y. Chen, Perfect invisibility concentrator with simplified material parameters, Front. Phys. **13**, 134101 (2018).
[24] A. Abdolali, H. Barati Sedeh, and M. H. Fakheri, Geometry free materials enabled by transformation optics for enhancing the intensity of electromagnetic waves in an arbitrary domain, J. Appl. Phys. **127**, 054902 (2020).
[25] H. Barati, M. Fakheri, and A. Abdolali, Experimental demonstration of metamaterial-assisted antenna beam deflection through folded transformation optics, J. Opt. **20**, 085101 (2018).
[26] H. B. Sedeh, M. H. Fakheri, and A. Abdolali, Advanced synthesis of meta-antenna radiation pattern enabled by transformation optics, J. Opt. **21**, 045108 (2019).
[27] D.-H. Kwon and D. H. Werner, Polarization splitter and polarization rotator designs based on transformation optics, Opt. Express **16**, 18731 (2008).
[28] Y. Ma, Y. Liu, M. Raza, Y. Wang, and S. He, Experimental Demonstration of a Multiphysics Cloak: Manipulating Heat Flux and Electric Current Simultaneously, Phys. Rev. Lett. **113**, 205501 (2014).
[29] G.-x. Yu, Y.-f. Lin, G.-q. Zhang, Z. Yu, L.-l. Yu, and J. Su, Design of square-shaped heat flux cloaks and concentrators using method of coordinate transformation, Front. Phys. China **6**, 70 (2011).
[30] R. Hu, S. Zhou, W. Shu, B. Xie, Y. Ma, and X. Luo, Directional heat transport through thermal reflection metadevice, AIP Adv. **6**, 125111 (2016).
[31] M. Farhat, P.-Y. Chen, S. Guenneau, and S. Enoch, *Transformation Wave Physics: Electromagnetics, Elastodynamics, and Thermodynamics* (Jenny Stanford Publishing, Singapore, 2016).
[32] F. Sun, Y. Liu, Y. Yang, Z. Chen, and S. He, Thermal surface transformation and its applications to heat flux manipulations, Opt. Express **27**, 33757 (2019).
[33] Y. Liu, F. Sun, and S. He, Fast adaptive thermal buffering by a passive open shell based on transformation thermodynamics, Adv. Theory Simul. **1**, 1800026 (2018).
[34] M. H. Fakheri, H. Barati Sedeh, and A. Abdolali, Omnidirectional perfect acoustic cloak realized by homogeneous materials, arXiv:1911.07073.
[35] F. Sun, Y. Liu, Y. Yang, Z. Chen, and S. He, Full space destructive interference by acoustic-null medium, Appl. Phys. Express **12**, 074003 (2019).
[36] A. Abdolali, A. Ashrafian, H. Barati Sedeh, and M. H. Fakheri, Scattering-free routing of surface plasmon polariton waves with optical null medium, arXiv:2006.07966.
[37] F. Sun and S. He, Optical surface transformation: Changing the optical surface by homogeneous optic-null medium at will, Sci. Rep. **5**, 16032 (2015).
[38] Q. He, S. Xiao, X. Li, and L. Zhou, Optic-null medium: Realization and applications, Opt. Express **21**, 28948 (2013).
[39] H. Barati Sedeh, M. H. Fakheri, A. Abdolali, and F. Sun, Experimental demonstration of an arbitrary shape dc electric concentrator, Sci. Rep. **10**, 16722 (2020).
[40] Y. Zhang, Y. Luo, J. Pendry, and B. Zhang, Transformation-Invariant Metamaterials, Phys. Rev. Lett. **123**, 067701 (2019).
[41] T. Yang, K. P. Vemuri, and P. R. Bandaru, Experimental evidence for the bending of heat flux in a thermal metamaterial, Appl. Phys. Lett. **105**, 083908 (2014).
[42] F. Chen and D. Y. Lei, Experimental realization of extreme heat flux concentration with easy-to-make thermal metamaterials, Sci. Rep. **5**, 11552 (2015).